


## Singly differential cross sections for direct scattering, electron capture, and ionization in proton-hydrogen collisions

C. T. Plowman<sup>✉</sup>, K. H. Spicer, I. B. Abdurakhmanov, A. S. Kadyrov<sup>✉,\*</sup>, and I. Bray<sup>✉</sup>  
*Curtin Institute for Computation and Department of Physics and Astronomy, Curtin University,  
 GPO Box U1987, Perth, WA 6845, Australia*

 (Received 24 July 2020; revised 16 October 2020; accepted 26 October 2020; published 12 November 2020)

We use the two-center wave-packet convergent close-coupling approach to calculate singly differential cross sections for direct scattering, electron capture, and ionization in proton-hydrogen collisions at intermediate energies. The distinct feature of the approach is that it gives a complete differential picture of all the interconnected processes at once, subject to the unitary principle. Results obtained for the angular differential cross sections of elastic scattering, excitation, and electron capture, as well as the ionization cross sections differential in the ejected-electron angle, and in the ejected-electron energy agree well with available experimental data. It is concluded that the two-center wave-packet convergent close-coupling approach is capable of providing a realistic differential picture of all collision processes taking place in proton-hydrogen collisions.

DOI: [10.1103/PhysRevA.102.052810](https://doi.org/10.1103/PhysRevA.102.052810)

### I. INTRODUCTION

Ion-atom collisions play a key role in laboratory and astrophysical plasmas. For example, such collisions find use in plasma diagnostics [1] and modeling [2], and spectroscopic analysis of distant supernovae [3]. In addition, better understanding of the physics of such collisions is paramount for hadron therapy [4]. As such, accurate modeling of the ion-atom collision system is very important. Many approaches have been developed to model ion-atom collisions [5]. Recent state-of-the-art reviews on energetic ion-atom and ion-molecule collisions can be found in Ref. [6].

As a particular example of an ion-atom scattering problem, the proton-hydrogen collision system has fundamental significance in scattering theory since it represents a genuine three-body problem where the interactions between all of the particles and the two-body bound-state wave functions in the reaction channels are analytically known. Therefore, proton scattering on hydrogen serves as a test bed for the development of various models.

In this work we focus on the intermediate energy region where projectile velocity is either comparable with, or somewhat larger than, the electron's orbital velocity. There are a number of methods applicable in the intermediate energy region. These are classical-trajectory Monte Carlo methods [7–9], a time-dependent density-functional theory [10], and approaches based on the close-coupling formalism like a basis-generator method [11], atomic-orbital close-coupling approaches [12–18], and lattice-based methods for direct solution of the time-dependent Schrödinger equation [19–21]. Most of these theoretical methods are capable of describing all collision processes taking place in the scattering system, namely, the elastic scattering, excitation, and ionization of the

target, and the electron capture by the projectile on a wide range of incident energies, including the entire keV region.

At sufficiently high projectile energies, the collisional times are short on the atomic timescale. For this reason, a perturbative treatment for the proton-hydrogen system becomes applicable. The process can be described using Born-type approximations where the proton is considered a small perturbation for the electronic wave function. Perturbative methods, such as the second-order Born approximation with corrected boundary conditions [22] and the three-body boundary-corrected continuum-intermediate-state (BCIS-3B) method [56], as well as continuum distorted-wave (CDW) approaches [23,24] have been developed.

The close-coupling approaches are not ideal for differential studies of high-energy collisions since the interaction matrix elements become highly oscillatory making numerical evaluation extremely difficult. Additionally, difficulties in modeling the continuum have historically restricted close-coupling approaches from finding applications in charge exchange processes, especially when the probability of electron capture into the continuum of the projectile cannot be ignored. Recently, three different implementations of the convergent close-coupling approach have been developed to circumvent these difficulties: the fully quantum-mechanical [25,26], standard semiclassical [27], and wave-packet semiclassical [28,29]. These approaches are based on two different types of pseudostates for discretization of the continuum of the target atom and the atom formed by the projectile after capturing the electron. The first two methods used a basis of Laguerre pseudostates, while the third used a basis obtained from combining eigenstates and continuum wave packets. Implementation of Laguerre- and wave-packet-pseudostate bases yielded excellent results for cross sections of various processes taking place in ion collisions with atomic hydrogen [25,27–30]. These approaches were mostly used to calculate integrated cross sections of various processes.

\*a.kadyrov@curtin.edu.au

Thus, as described above, a great number of theoretical methods have been developed to treat ion-atom collisions. Most of these methods were successful in describing the less-detailed integrated cross sections. However, only a few of them were applied to study the problem on a more-detailed differential level. When applied, they may lead to incorrect results on the differential level despite giving very good results for the integrated cross sections. For instance, as mentioned by Kerby *et al.* [31], while very good agreement is found between CDW-EIS and the experimental data on the total ionization cross section in a wide range of impact energies, the CDW-EIS does not reproduce the measured singly and doubly differential cross sections well and, therefore, the agreement with the total ionization cross section must be considered to be fortuitous. Moreover, each of those methods applied to calculate differential cross sections tackled only one particular aspect of the problem. For example, the second-order Born approximation with corrected boundary conditions [22] was very successful in describing differential electron capture, however, it cannot be applied to differential ionization. The aforementioned atomic-orbital close-coupling and lattice-based approaches have not been applied to calculate differential cross sections of various processes taking place in ion-atom collisions.

Here, the main goal is to use the wave-packet convergent close-coupling (WP-CCC) approach to calculate singly differential cross sections (SDCS) for direct scattering, electron capture and ionization in proton-hydrogen collisions in the intermediate energy region in a unified fashion. The distinct feature of the approach is that it gives a complete differential picture of all the interconnected processes at once, subject to the unitary principle. Previously, the wave-packet implementation of the convergent close-coupling approach has been used to calculate various integrated cross sections for proton collisions with hydrogen in the ground [32] and excited [33] states. The approach has also been applied to calculate the doubly differential ionization cross sections [29]. Here we report angular differential cross sections for elastic scattering, excitation into  $n = 2$  states (here,  $n$  is the principal quantum number of the atom in the final state) and electron capture. Ionization cross sections differential in ejected electron angle and energy are also calculated.

Unless specified otherwise, atomic units are used throughout this manuscript.

## II. TWO-CENTER WAVE-PACKET CONVERGENT CLOSE-COUPPLING METHOD

Various aspects of the two-center wave-packet convergent close-coupling method for ion-atom collisions are described in detail in our earlier works [29,32,33]. The approach has been extended to multicharged projectiles in Refs. [34,35] and to two-electron targets in Ref. [36]. A brief description of the method is given here with emphasis on the parts relevant to the present calculations.

### A. Close-coupling formalism

We consider scattering of a proton on the hydrogen atom. This three-body Coulomb scattering problem is governed by

the full three-body Schrödinger equation for the total scattering wave function

$$(H - E)\Psi_i^+ = 0, \quad (1)$$

with the outgoing-wave boundary conditions, where  $E$  is the total energy and  $H$  is the full three-body Hamiltonian of the collision system. Index  $i$  denotes the initial channel, from which the total scattering wave develops. In the present work it is taken to be the projectile of energy  $E_i$  incident on H in the ground state. Equation (1) is solved by expanding the total scattering wave function in terms of the target ( $\psi_\alpha$ ) and projectile ( $\psi_\beta$ ) centered pseudostates as

$$\Psi_i^+ \approx \sum_{\alpha=1}^N F_\alpha(t, \mathbf{b}) \psi_\alpha(\mathbf{r}_t) e^{iq_\alpha \cdot \rho} + \sum_{\beta=1}^M G_\beta(t, \mathbf{b}) \psi_\beta(\mathbf{r}_p) e^{iq_\beta \cdot \sigma}, \quad (2)$$

where  $F_\alpha$  and  $G_\beta$  are time-dependent coefficients, and  $N$  and  $M$  are the numbers of basis functions on the target and projectile centers. The expansion given in Eq. (2) is written in the Jacobi coordinates, where index  $\alpha$  denotes a quantum state in a channel where a projectile of relative momentum  $\mathbf{q}_\alpha$  is incident on a bound state of the target atom. Index  $\beta$  denotes a quantum state in the rearrangement channel where the atom formed by the projectile after electron capture has momentum  $\mathbf{q}_\beta$  relative to the stripped target nucleus. The position of the projectile with respect to the center of mass of the target nucleus-electron pair is denoted by  $\rho$ , while  $\sigma$  is the position of the projectile-electron pair with respect to the target nucleus.  $\mathbf{R}$  represents the position vector of the projectile relative to the target nucleus. In this work we assume that the target nucleus is located at a fixed origin and the projectile is moving along a straight-line classical trajectory  $\mathbf{R} = \mathbf{b} + \mathbf{v}t$ , where  $\mathbf{b}$  is the impact parameter and  $\mathbf{v}$  is the projectile velocity. The impact parameter is defined so that  $\mathbf{b} \cdot \mathbf{v} = 0$  and the  $z$  axis is chosen parallel to  $\mathbf{v}$ . The position of the electron relative to the target proton is  $\mathbf{r}_t$ , while  $\mathbf{r}_p$  is the electron position relative to the projectile. The full Hamiltonian is given by the sum of the free three-particle Hamiltonian and the interaction potential between each of the particles,

$$H = H_0 + V, \quad (3)$$

where  $H_0$  is expressed in the target and projectile centers, respectively, as

$$H_0 = \frac{1}{2\mu} \nabla_\rho^2 - \frac{1}{2} \nabla_{r_t}^2 = -\frac{1}{2\mu} \nabla_\sigma^2 - \frac{1}{2} \nabla_{r_p}^2, \quad (4)$$

where  $\mu$  is the reduced mass of the proton-hydrogen system. The interaction potential is given by the sum of the electron-target, electron-projectile, and nucleus-nucleus interactions,

$$V = \frac{1}{R} - \frac{1}{r_t} - \frac{1}{r_p}. \quad (5)$$

The set of projectile (and target) centered pseudostates is constructed from negative-energy eigenstates of the hydrogen atom and positive-energy wavepacket pseudostates generated by discretizing the continuum into  $N_c$  nonoverlapping subintervals up to momentum,  $\kappa_{\max}$ . The radial part of the  $n$ th pseudostate wave function is given by integrating the

Coulomb wave over the corresponding momentum bin,

$$\phi_{nl}(r) = \frac{1}{\sqrt{\kappa_n - \kappa_{n-1}}} \int_{\kappa_{n-1}}^{\kappa_n} d\kappa U_l(\kappa, r). \quad (6)$$

Together, the negative-energy eigenstates and positive-energy pseudostates of the target are orthogonal to one another and diagonalise the atomic hydrogen Hamiltonian,

$$\langle \psi_{\alpha'} | \psi_{\alpha} \rangle = \delta_{\alpha'\alpha}, \quad \langle \psi_{\alpha'} | H_{\alpha} | \psi_{\alpha} \rangle = \delta_{\alpha'\alpha} \varepsilon_{\alpha}. \quad (7)$$

Here  $\varepsilon_{\alpha}$  is the energy of the target state, which is the eigenvalue for negative-energy states and

$$\varepsilon_n = \frac{\kappa_n^2 + \kappa_n \kappa_{n-1} + \kappa_{n-1}^2}{6} \quad (8)$$

for wavepacket pseudostates. Similarly, the projectile pseudostates satisfy

$$\langle \psi_{\beta'} | \psi_{\beta} \rangle = \delta_{\beta'\beta}, \quad \langle \psi_{\beta'} | H_{\beta} | \psi_{\beta} \rangle = \delta_{\beta'\beta} \varepsilon_{\beta}. \quad (9)$$

However, the target-centered pseudostates are not orthogonal to the projectile-centered pseudostates.

Substituting the expansion in Eq. (2) into the Schrödinger equation and applying the Hamiltonian operator we obtain the following set of first-order differential equations for the time-dependent coefficients,

$$\begin{aligned} i\dot{F}_{\alpha'} + i \sum_{\beta=1}^M \dot{G}_{\beta} \tilde{K}_{\alpha'\beta} &= \sum_{\alpha=1}^N F_{\alpha} D_{\alpha'\alpha} + \sum_{\beta=1}^M G_{\beta} \tilde{Q}_{\alpha'\beta}, \\ i \sum_{\alpha=1}^N \dot{F}_{\alpha} K_{\beta'\alpha} + i\dot{G}_{\beta'} &= \sum_{\alpha=1}^N F_{\alpha} Q_{\beta'\alpha} + \sum_{\beta=1}^M G_{\beta} \tilde{D}_{\beta'\beta}, \\ \alpha' &= 1, 2, \dots, N, \quad \beta' = 1, 2, \dots, M, \end{aligned} \quad (10)$$

where dots over  $F_{\alpha}$  and  $G_{\beta}$  denote time derivatives. Here we have used the semiclassical approximation [5] to simplify the expansion resulting from operating  $H$  on  $\Psi_i^+$  (see Ref. [29] for details). The overlap integrals in Eq. (10) are given as

$$\begin{aligned} K_{\beta'\alpha}(\mathbf{R}) &= \langle \psi_{\beta'} | \exp[-i\mathbf{v} \cdot \mathbf{r}_i] | \psi_{\alpha} \rangle \\ &\times \exp[iv^2 t/2 + i(\varepsilon_{\beta'} - \varepsilon_{\alpha})t], \end{aligned} \quad (11)$$

$$\begin{aligned} \tilde{K}_{\alpha'\beta}(\mathbf{R}) &= \langle \psi_{\alpha'} | \exp[i\mathbf{v} \cdot \mathbf{r}_i] | \psi_{\beta} \rangle \\ &\times \exp[-iv^2 t/2 + i(\varepsilon_{\alpha'} - \varepsilon_{\beta})t]. \end{aligned} \quad (12)$$

Direct-scattering matrix elements are given as

$$D_{\alpha'\alpha}(\mathbf{R}) = \langle \psi_{\alpha'} | \bar{V}_{\alpha} | \psi_{\alpha} \rangle \exp[i(\varepsilon_{\alpha'} - \varepsilon_{\alpha})t], \quad (13)$$

$$\tilde{D}_{\beta'\beta}(\mathbf{R}) = \langle \psi_{\beta'} | \bar{V}_{\beta} | \psi_{\beta} \rangle \exp[i(\varepsilon_{\beta'} - \varepsilon_{\beta})t], \quad (14)$$

where  $\bar{V}_{\alpha} = Z_t Z_p / R - Z_p / r_p$  and  $\bar{V}_{\beta} = Z_t Z_p / R - Z_t / r_t$ . Electron-transfer matrix elements are given as

$$\begin{aligned} Q_{\beta'\alpha}(\mathbf{R}) &= \langle \psi_{\beta'} | \exp[-i\mathbf{v} \cdot \mathbf{r}_i] (H_{\alpha} + \bar{V}_{\alpha} - \varepsilon_{\alpha}) | \psi_{\alpha} \rangle \\ &\times \exp[iv^2 t/2 + i(\varepsilon_{\beta'} - \varepsilon_{\alpha})t], \end{aligned} \quad (15)$$

$$\begin{aligned} \tilde{Q}_{\alpha'\beta}(\mathbf{R}) &= \langle \psi_{\alpha'} | \exp[i\mathbf{v} \cdot \mathbf{r}_i] (H_{\beta} + \bar{V}_{\beta} - \varepsilon_{\beta}) | \psi_{\beta} \rangle \\ &\times \exp[-iv^2 t/2 + i(\varepsilon_{\alpha'} - \varepsilon_{\beta})t], \end{aligned} \quad (16)$$

where  $H_{\alpha}$  and  $H_{\beta}$  are the target and projectile atom Hamiltonians. Thus, starting from the exact Schrödinger equation and using a different ansatz for the total scattering wave function, we arrived at the same set of equations for the expansion coefficients as that obtained in the conventional close-coupling approach [5].

The expansion coefficients  $F_{\alpha}(t, \mathbf{b})$  and  $G_{\beta}(t, \mathbf{b})$  as  $t \rightarrow +\infty$  represent the probability amplitudes (in the impact-parameter representation) of transitions into the target and projectile pseudostates and as  $t \rightarrow -\infty$  satisfy the initial boundary condition

$$\begin{aligned} F_{\alpha}(-\infty, \mathbf{b}) &= \delta_{\alpha 1}, \quad \alpha = 1, 2, \dots, N, \\ G_{\beta}(-\infty, \mathbf{b}) &= 0, \quad \beta = 1, 2, \dots, M. \end{aligned} \quad (17)$$

The direct-scattering matrix elements are calculated in the spherical coordinates, while the overlap integrals and the electron-transfer matrix elements are evaluated using the spheroidal coordinates as described in Ref. [25]. The existing computational code, which solves Eq. (10), has been modified to run on GPU based supercomputers which reduced the computational time by orders of magnitude. Offloading computation of the direct, overlap and electron-transfer matrix elements to GPUs is achieved through utilization of the OpenACC directives recently introduced to Fortran [37], while the CUDA library, *cuSolverDn* [38], is used to solve the system of linear equations emerging at each time step of the Runge-Kutta propagation.

Once the expansion coefficients  $F_{\alpha}(t, \mathbf{b})$  and  $G_{\beta}(t, \mathbf{b})$  have been found in the asymptotic state (as  $t \rightarrow +\infty$ ) the integrated cross sections for all included electronic transitions can be calculated using the technique described in Ref. [29]. However, for the differential cross sections we first need to obtain the scattering amplitudes in terms of the expansion coefficients.

## B. Scattering amplitudes

In addition to the integrated cross sections, the present WP-CCC approach also allows us to calculate all types of differential ionization cross sections including the fully differential one. This can be realized due to the feature of the wave-packet bin states describing the continuum.

According to Refs. [39,40], the momentum-space scattering amplitude of any process taking place in proton collisions with atomic hydrogen is written in terms of the total scattering wave function  $\Psi_i^+$  as

$$T_{fi}(\mathbf{q}_f, \mathbf{q}_i) = \langle \Phi_f^- | \overleftarrow{H} - E | \Psi_i^+ \rangle, \quad (18)$$

where  $\Phi_f^-$  is the asymptotic state corresponding to the final channel and  $\mathbf{q}_i$  and  $\mathbf{q}_f$  are the relative momentum in the initial and final channel, respectively. The arrow over the total three-body Hamiltonian operator  $H$  indicates the direction of its action. Eq. (18) is general and applicable for all processes including direct scattering, electron transfer and ionization. To be able to calculate various integrated and differential cross sections, we have to determine the scattering amplitude  $T_{fi}(\mathbf{q}_f, \mathbf{q}_i)$  defined in Eq. (18) in terms of the scattering amplitudes in the impact-parameter representation introduced in Sec. II A.

If the result of the scattering is excitation of the target, then  $\Phi_f^-$  is given as a product of a plane wave describing the scattered projectile and a bound state wave function of the target in the final state. The latter is written as  $e^{i\mathbf{q}_\alpha \cdot \mathbf{r}_\alpha} \psi_\alpha(\mathbf{r}_\alpha)$  with  $\alpha = f$ . Then, Eq. (18) gives the direct scattering (DS) amplitude

$$T_{fi}^{\text{DS}}(\mathbf{q}_f, \mathbf{q}_i) = \langle \mathbf{q}_f \psi_f | \overleftarrow{H} - E | \Psi_i^+ \rangle. \quad (19)$$

Only when the final state is a negative-energy eigenstate of the target atom does Eq. (19) reduce to the well-known form of  $T_{fi}^{\text{DS}}(\mathbf{q}_f, \mathbf{q}_i) = \langle \mathbf{q}_f \psi_f | \overline{V}_\alpha | \Psi_i^+ \rangle$ .

For electron capture into the bound states of the projectile,  $\Phi_f^-$  is a product of the plane wave corresponding to the relative motion of the target nucleus with the bound states of the atom formed by the projectile in the final state. It is written as  $e^{i\mathbf{q}_\beta \cdot \mathbf{r}_\beta} \psi_\beta(\mathbf{r}_\beta)$  with  $\beta = f$ . Then Eq. (18) gives the electron capture (EC) amplitude

$$T_{fi}^{\text{EC}}(\mathbf{q}_f, \mathbf{q}_i) = \langle \mathbf{q}_f \psi_f | \overleftarrow{H} - E | \Psi_i^+ \rangle. \quad (20)$$

When the final state is a negative-energy eigenstate of the projectile atom, Eq. (20) reduces to  $T_{fi}^{\text{EC}}(\mathbf{q}_f, \mathbf{q}_i) = \langle \mathbf{q}_f \psi_f | \overline{V}_\beta | \Psi_i^+ \rangle$ .

Treatment of scattering processes where the electron remains bound to either the target or the projectile is computationally simpler than the process leading to three unbound particles. When the final state corresponds to breakup,  $\Phi_f^-$  is the three-body Coulomb asymptotic state described by incoming waves representing the three unbound particles in the final state [41,42]. However, since our approach is based on the expansion of  $\Psi_i^+$  in terms of square-integrable target and projectile pseudostates, we do not need the three-body Coulomb asymptotic state. In order to derive the breakup amplitude we use the idea developed in Ref. [43].

According to this idea, the ionization amplitude can be found by projecting the Coulomb wave describing the final ionized state of the electron onto the two-center scattering wave function. Since the wave-packet bin states themselves are constructed from the Coulomb wave function, this procedure becomes much simpler. Full details of the WP-CCC approach to differential ionization is given in Ref. [29]. Here, we only give the final result. The amplitude for direct ionization (DI) of the target atom is written as

$$T_{fi}^{\text{DI}}(\boldsymbol{\kappa}, \mathbf{q}_f, \mathbf{q}_i) = \langle \varphi_\kappa | \psi_f \rangle T_{fi}^{\text{DS}}(\mathbf{q}_f, \mathbf{q}_i), \quad (21)$$

where  $\varphi_\kappa$  is the true Coulomb wave representing the continuum state of the ejected electron with momentum  $\boldsymbol{\kappa}$  relative to the target nucleus. Thus we see that the DI amplitude is given in terms of the amplitude for excitation of the corresponding positive-energy pseudostate.

The amplitude for electron capture into continuum (ECC) of the atom formed by the projectile can be written as

$$T_{fi}^{\text{ECC}}(\boldsymbol{\varkappa}, \mathbf{q}_f, \mathbf{q}_i) = \langle \varphi_\varkappa | \psi_f \rangle T_{fi}^{\text{EC}}(\mathbf{q}_f, \mathbf{q}_i), \quad (22)$$

where  $\boldsymbol{\varkappa}$  is the momentum of the ejected electron relative to the projectile nucleus. Thus we get that the ECC amplitude is given in terms of the amplitude for electron capture into the corresponding positive-energy pseudostate.

The direct scattering amplitudes  $T_{fi}^{\text{DS}}(\mathbf{q}_f, \mathbf{q}_i)$  (for elastic scattering, and excitation to either negative-energy

eigenstates or positive-energy pseudostates) are calculated from the impact-parameter space transition probability amplitudes as follows:

$$\begin{aligned} T_{fi}^{\text{DS}}(\mathbf{q}_f, \mathbf{q}_i) &= \frac{1}{2\pi} \int d\mathbf{b} e^{i\mathbf{q}_\perp \cdot \mathbf{b}} \mathcal{T}_{fi}^{\text{DS}}(\mathbf{b}) \\ &= iv \int d\mathbf{b} e^{i\mathbf{q}_\perp \cdot \mathbf{b}} [F_f(+\infty, \mathbf{b}) - \delta_{fi}] \\ &= 2\pi iv e^{im\phi_f} \int_0^\infty db b [\tilde{F}_f(+\infty, b) - \delta_{fi}] J_m(q_\perp b), \end{aligned} \quad (23)$$

where  $\mathbf{q}_\perp$  is the perpendicular component of the momentum transfer  $\mathbf{q} = \mathbf{q}_i - \mathbf{q}_f$ ,  $\mathcal{T}_{fi}^{\text{DS}}(\mathbf{b})$  is the direct scattering amplitude in the impact-parameter representation,  $\tilde{F}_f(t, b) = e^{im\phi_b} F_f(t, \mathbf{b})$ ,  $m$  is the magnetic quantum number of the bound state in the final channel,  $\phi_f$  is the azimuthal angle of  $\mathbf{q}_f$ , and  $J_m$  is the Bessel function of the  $m$ th order.

The electron capture amplitudes  $T_{fi}^{\text{EC}}(\mathbf{q}_f, \mathbf{q}_i)$  (for electron transfer into either negative-energy eigenstates or positive-energy pseudostates of the projectile atom) are related to the impact-parameter space transition probability amplitudes as follows:

$$\begin{aligned} T_{fi}^{\text{EC}}(\mathbf{q}_f, \mathbf{q}_i) &= \frac{1}{2\pi} \int d\mathbf{b} e^{i\mathbf{q}_\perp \cdot \mathbf{b}} \mathcal{T}_{fi}^{\text{EC}}(\mathbf{b}) \\ &= iv \int d\mathbf{b} e^{i\mathbf{q}_\perp \cdot \mathbf{b}} G_f(+\infty, \mathbf{b}) \\ &= 2\pi iv e^{im\phi_f} \int_0^\infty db b \tilde{G}_f(+\infty, b) J_m(q_\perp b), \end{aligned} \quad (24)$$

where  $\mathcal{T}_{fi}^{\text{DS}}(\mathbf{b})$  is the electron-capture amplitude in the impact-parameter representation and  $\tilde{G}_f(t, b) = e^{im\phi_b} G_f(t, \mathbf{b})$ . The integrals entering Eqs. (23) and (24) are accurately calculated using the Gauss-Legendre quadrature method. Specifically, 64 points were used from  $b_{\min} = 0$  to  $b_{\max} = 14$  au for angular differential cross sections (Sec. III A) and 128 points from  $b_{\min} = 0$  to  $b_{\max} = 48$  au for angular and energy differential cross sections for ionization (Sec. III B).

We note that Eq. (22) is written in the frame of coordinates associated with the projectile. In order to combine the DI and ECC amplitudes, we need to bring the two into a common frame of reference. A laboratory frame of coordinates used in the experiment will be adopted as a common frame of reference. The electron momentum  $\boldsymbol{\varkappa}$  and the momentum transfer  $\mathbf{q}$  in the projectile frame correspond to  $\boldsymbol{\kappa} - \mathbf{v}$  and  $\mathbf{q} - \boldsymbol{\kappa}$  in the laboratory frame, respectively. The transformation of the amplitudes representing the electron-capture process is performed in the following way. First, the electron-capture amplitudes are calculated using Eq. (24) with  $\mathbf{q}_\perp$  being substituted with  $(\mathbf{q} - \mathbf{v})_\perp$ . This gives us amplitudes for electron capture into the projectile continuum with momentum  $\boldsymbol{\varkappa}$ , which can only take certain values predefined by the employed basis of wavepacket pseudostates. This corresponds to certain values and directions of  $\boldsymbol{\kappa}$ . All other required values and directions are obtained using interpolation.



### C. Cross sections

Once the time-dependent coefficients in Eq. (10) are found, the differential cross section for the transition from the initial state  $i$  to the final state  $f$  is calculated as

$$\frac{d\sigma_{fi}^{\text{DS(EC)}}}{d\Omega_f} = \frac{\mu^2}{(2\pi)^2} \frac{q_f}{q_i} |T_{fi}^{\text{DS(EC)}}(\mathbf{q}_f, \mathbf{q}_i)|^2, \quad (25)$$

where  $\mu$  is the reduced mass of the collision system and  $\Omega_f$  is the solid angle of  $\mathbf{q}_f$  (relative to  $\mathbf{q}_i$ ).

In addition to the angular differential cross sections for direct scattering and electron capture, in this paper we also present the singly differential cross sections for ionization. In particular, we focus on the ionization cross sections differential in the energy of the ejected electron and in the angle of the ejected electron, measured in the experiment [31]. These cross sections can be calculated from the fully differential cross section as

$$\frac{d\sigma_{\text{ion}}}{dE_e} = \int \frac{d^3\sigma_{\text{ion}}}{dE_e d\Omega_e d\Omega_f} d\Omega_f d\Omega_e, \quad (26)$$

and

$$\frac{d\sigma_{\text{ion}}}{d\Omega_e} = \int \frac{d^3\sigma_{\text{ion}}}{dE_e d\Omega_e d\Omega_f} d\Omega_f dE_e, \quad (27)$$

where  $\Omega_e$  is the solid angle of  $\boldsymbol{\kappa}$ , the electron momentum, into which the electron is ejected and  $E_e$  is the ejected electron energy. In the current two-center approach the fully differential cross section for ionization consists of the incoherent combination of the direct ionization and electron-capture into continuum components [44]. In the laboratory frame it is written as

$$\begin{aligned} \frac{d^3\sigma_{\text{ion}}}{dE_e d\Omega_e d\Omega_f} = & \frac{\mu^2}{(2\pi)^2} \frac{q_f \kappa}{q_i} (|T_{fi}^{\text{DI}}(\boldsymbol{\kappa}, \mathbf{q}_f, \mathbf{q}_i)|^2 \\ & + |T_{fi}^{\text{ECC}}(\boldsymbol{\kappa} - \mathbf{v}, \mathbf{q}_f, \mathbf{q}_i)|^2). \end{aligned} \quad (28)$$

The ionization amplitudes  $T_{fi}^{\text{DI}}(\boldsymbol{\kappa}, \mathbf{q}_f, \mathbf{q}_i)$  and  $T_{fi}^{\text{ECC}}(\boldsymbol{\kappa} - \mathbf{v}, \mathbf{q}_f, \mathbf{q}_i)$  are expressed in terms of the time-dependent coefficients  $F_f(t, \mathbf{b})$  and  $G_f(t, \mathbf{b})$  in the asymptotic region,  $t \rightarrow +\infty$ , respectively, as described in Sec. II B. A cross section differential in a particular variable is obtained by integrating the fully differential cross section over all other variables.

### III. CALCULATIONS OF SINGLY DIFFERENTIAL CROSS SECTIONS

The set of Eqs. (10) for the expansion coefficients, representing the transition amplitudes, was solved using the Runge-Kutta method by incrementing the position of the projectile along the  $z = v_0 t$  axis in the scattering plane from  $z_{\text{min}} = -300$  au to  $z_{\text{max}} = 300$  au for all impact parameters. The  $z$  grid was discretized using 1200 points. The impact parameters ranged from 0 up to 48 au, which was sufficient to allow for the probability of all processes being investigated to fall off several orders of magnitude. Additional impact parameters made no significant contribution to the results. For discretization of the continuum, the maximum momentum  $\kappa_{\text{max}}$  was increased systematically until no further change

in the results was observed. More specific energy-dependent values are given below.

#### A. Angular differential cross sections for elastic scattering, $n = 2$ excitation, and electron capture

Angular differential cross sections for elastic scattering, excitation into the  $n = 2$  states, where  $n$  is the principal quantum number of the atom in the final state, and electron capture (summed over all included projectile bound states) were calculated from the transition amplitudes for the corresponding states for each of these processes. It was found that a basis containing  $10 - \ell$  bound states and 20 bin states (for each orbital angular momentum  $\ell$ ), on both centers, with the maximum orbital angular momentum  $\ell_{\text{max}} = 3$  was sufficient to obtain convergence in the differential cross sections at all three energies considered. The maximum ionization state energy was set by momenta  $\kappa_{\text{max}}$  of 5.5 au which was verified to be sufficient for all the angular differential cross sections considered in this work to converge at intermediate energies. In calculating the angular SDCS over the range from  $\theta_{\text{min}} = 0$  mrad to  $\theta_{\text{max}} = 3.5$  mrad, it was found that including additional impact parameters beyond  $b_{\text{max}} = 14$  au made no appreciable difference to the SDCS. While 64 impact parameter points in a Gaussian-Legendre distribution were sufficient for most results, 128 points were required to remove unphysical oscillations in the differential cross section for  $n = 2$  excitation at 125 keV. Surprisingly, to obtain agreement between the total cross section calculated the standard way (see Ref. [29]) and the value resulting from integrating the corresponding SDCS for the three processes considered, it was necessary to include a wide range of scattering angles. Specifically, scattering angles as large as 20 mrad were needed to obtain agreement within 1%.

The results obtained using the WP-CCC approach are presented in Fig. 1 in comparison with experimental data [45–47] and other calculations [22,48–56]. Following the experimental work, the cross sections are given in the center-of-mass frame (where the center of mass of the proton-hydrogen system is at rest). The WP-CCC results agree well with experiment for all three processes.

The present elastic-scattering calculations agree well with most of the literature while agreeing best with results from the multichannel optical-potential approach of Potvliege *et al.* [52]. However, there is disagreement with the results of the impact-parameter Faddeev approach by Alt *et al.* [48] at 60 keV and a partial-wave-expansion approach by Wong *et al.* [54] at 25 and 60 keV. The Faddeev approach deviates from other calculations at scattering angles below 0.5 mrad possibly due to insufficient number of channels included in Ref. [48]. The elastic-scattering cross section by Wong *et al.* [54], obtained in a partial-wave expansion approach using only the ground state of H, substantially overestimates the experimental data above 1 mrad at 25 keV and below 1 mrad at 60 keV.

Henne *et al.* [50] used a doorway approximation within the optical-potential method to calculate differential excitation into the  $n = 2$  states. Their results are available at 25 and 60 keV and tend to underestimate the experiment [46] near the

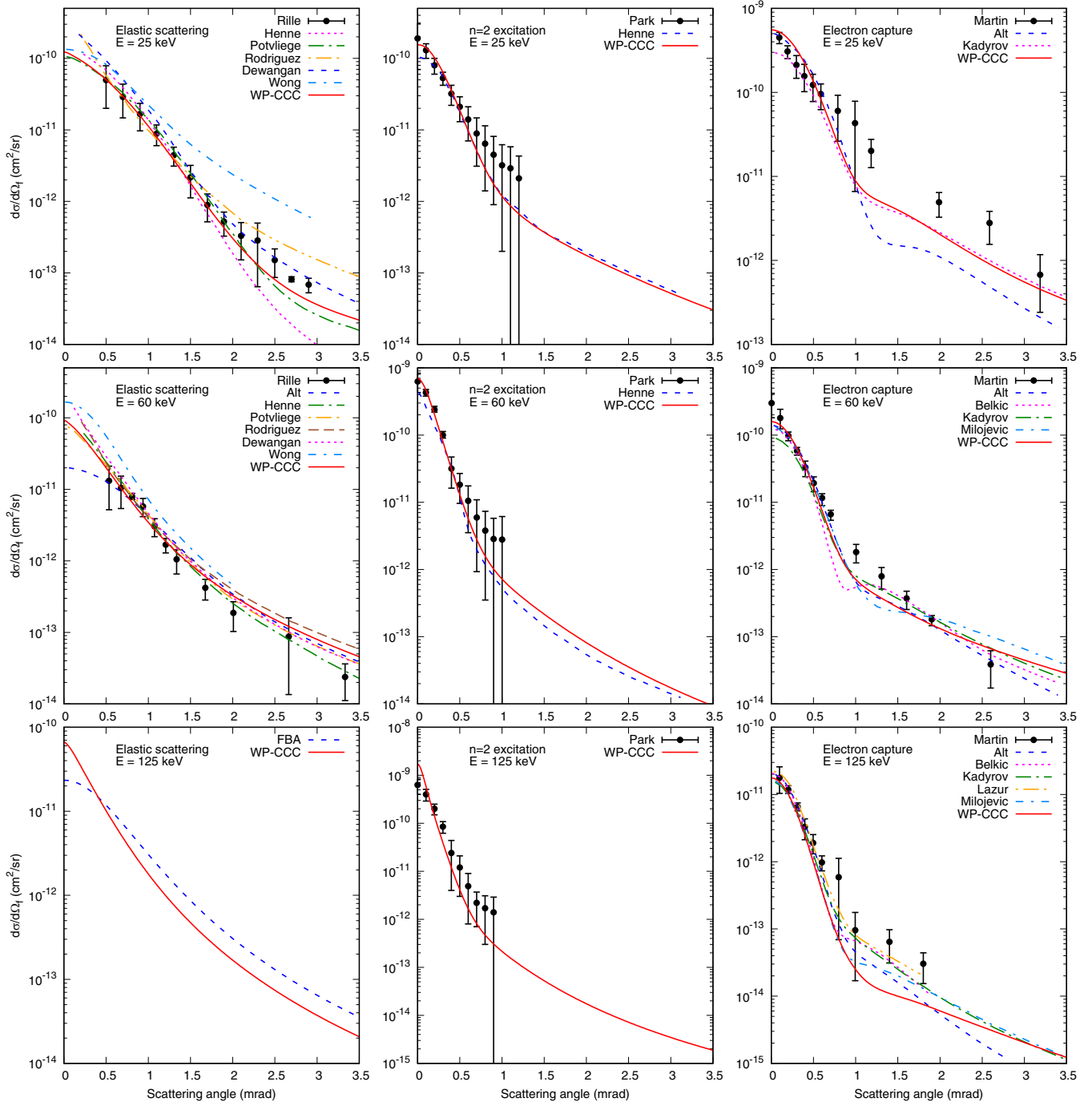


FIG. 1. Angular differential cross sections (in the center-of-mass frame) for elastic scattering,  $n = 2$  excitation, and electron capture in proton-hydrogen collisions at 25, 60, and 125 keV. Electron capture results are summed over all negative-energy pseudostates in the projectile basis (i.e., 10 s, 9 p, 8 d, and 7 f states). Experimental data are by Rille *et al.* [45], Park *et al.* [46], and Martin *et al.* [47] for elastic scattering, excitation, and electron capture, respectively. The theoretical results are: the present WP-CCC approach; impact-parameter Faddeev approach of Alt *et al.* [48]; second-order boundary-corrected Born approximation of Belkić [22]; Glauber approximation by Dewangan and Eichler [49]; doorway approximation to optical potential by Henne *et al.* [50]; a three-dimensional integral equation approach by Kadyrov *et al.* [51]; multichannel optical potential approach by Potvliege *et al.* [52]; eikonal-Glauber approximation by Rodriguez [53]; partial-wave approach by Wong *et al.* [54]; Dodd-Greider approach by Lazur *et al.* [55]; three-body boundary-corrected continuum-intermediate-state method Milojević *et al.* [56].

forward direction. This should lead to significant underestimation of the corresponding integrated cross section.

Angular differential cross sections for electron capture generally agree well with experiment. However, the WP-CCC

differential cross section is noticeably smaller at projectile energies of 25 and 125 keV for scattering angles from 1.5 to 2 mrad. The electron capture results agree best with those calculated using a three-dimensional integral equation

approach [51] at 25 and 60 keV. A recently developed approach based on the first iteration of the Dodd-Greider equations by Lazur *et al.* [55] appears to perform well for electron capture at 125 keV; however, results at 25 and 60 keV are not available. Also, it is unclear if the approach can provide the cross sections for direct scattering and ionization. A recent extension of the BCIS-3B method to include capture into many bound states by Milojević *et al.* [56] agrees well with our results below 1 mrad at both 60 and 125 keV. However, between 1 and 1.5 mrad it is smaller and beyond 2 mrad it is larger than the other theoretical results for 60 keV projectiles. At 125 keV the BCIS-3B results are closer to experiment from 1 to 2 mrad than the WP-CCC results but towards larger angles they converge. Note that all the theoretical calculations mentioned above, except the present WP-CCC ones and the recent BCIS-3B calculations, are for electron capture into the ground state of hydrogen. These are scaled up by a factor of 1.202 to effectively compensate for the missing excited states. Note that in our calculations the ground-state of the projectile atom contributes 71% of the total electron capture cross section, indicating the inclusion of additional negative-energy exchange channels has a significant effect on the results.

Our trial calculations at projectile energies in the MeV region have reproduced the Thomas peak [57] in the angular differential cross section for electron capture and described the experiment [58] reasonably well. This suggests our approach is capable of modeling the multiple-scattering mechanism responsible for the Thomas mechanism. Similar close-coupling calculations were performed by Toshima and Eichler using  $s$  states on both centers [59] and  $s$  states on one center and  $s$ ,  $p$  and  $d$  states on the other center [60]. Despite using a Gaussian basis (which allows one to obtain all transition matrix elements in an analytical form), these authors were not able to obtain convergent results. We have reproduced these results with similar bases as those used by Toshima and Eichler. However, at this stage we were not able to achieve the same level of convergence as in the other cross sections reported here for lower energies, when a large two-center basis is used and the angular momentum of the included states is increased. This was due to the electron-transfer matrix elements becoming highly oscillatory at high energies making numerical evaluations extremely difficult. For this reason, the results are not shown. Further work on optimizing the calculations of the electron-transfer matrix elements are required to achieve convergence in the high-energy regime.

### B. Angular and energy differential cross sections for ionization

For ionization calculations, the maximum momentum,  $\kappa_{\max}$ , of the included pseudostates was 5.0 au for projectile energies of 20, 48, and 67 keV. For projectile energies of 95 and 114 keV,  $\kappa_{\max}$  was set to 6.6 and 7.6 au, respectively. Additionally, impact parameters up to 48 au were found to be necessary to obtain convergence in both angular and energy differential cross sections and also 99% agreement between the integrated SDCSs and the total cross section for ionization. This is a significantly wider range than for nonbreakup scattering where accurate SDCS could be obtained considering angles up to 3.5 mrad and a maximum impact parameter of 14 au. A basis of  $5 - \ell$  bound states and 30 continuum

pseudostates for each orbital angular momentum quantum number  $\ell$ , on both centers, with  $\ell_{\max} = 4$  was found to be sufficient to obtain convergent differential cross sections at 25 keV. For higher projectile energies, a basis of  $10 - \ell$  bound states and 20 continuum pseudostates with  $\ell_{\max} = 3$  was sufficient.

The present calculations for the singly differential ionization cross sections in the ejected electron angle and energy are shown in Fig. 2 in comparison with the experiment by Kerby *et al.* [31] and other calculations [31,61–63] for several collision energies indicated in the legends. The results are shown in the laboratory frame where the target is at rest. The cross sections differential in the ejected electron angle are displayed in the left panels. There is significant variation between the different theoretical calculations. The present results agree very well with the experimental data at all the available projectile energies. The classical trajectory Monte Carlo (CTMC) and CDW-EIS results of Kerby *et al.* [31] are denoted as I and II, respectively. Generally, our results agree better with the CDW-EIS calculations. Theoretical results of Reading *et al.* [61] available only at the projectile energy of 20 keV are also shown. These authors used a finite Hilbert basis-set (FHBS) approach to obtain converged results with pseudostates up to  $\ell_{\max} = 5$ . Their cross section agrees well with the experiment and our results for the ejection angles from 20 to 90 deg. However, beyond 90 deg the FHBS results rise too quickly suggesting they converged to an incorrect result.

The right panels in Fig. 2 show results for ionization cross section differential in the ejected electron energy. Generally, there is again very good agreement between the present results and the experiment except for somewhat odd-looking points at 67 and 95 keV incident energies when energetic electrons are ejected. One can see a small bump in the WP-CCC results at the 20 and 48 keV incident energies and small ejection energies. This occurs when the contribution from direct ionization drops sharply as the ejection energy rises while the contribution from electron capture into the continuum increases (see Fig. 3). This feature washes out as collision energy goes up and is barely noticeable already at 67 keV.

The FHBS calculations for the energy-differential ionization cross section by Fu [62] (denoted as Fu I) and Fu *et al.* [63] (denoted as Fu II) are only available for small ejected electron energies where they agree well with the experimental results. However, they start deviating from the experiment rising too quickly above 20 eV at the collision energy of 20 keV and falling too sharply above 30 eV at 114 keV, further supporting our claim that the FHBS calculations of the Texas A&M group converged to a wrong result. As for the other results, the CTMC and CDW-EIS calculations of Kerby *et al.* [31] are denoted as I and II, respectively. Again, our results agree better with the CDW-EIS calculations. Note that at 67 keV both CTMC and CDW-EIS approaches of Kerby *et al.* [31] agree with our results suggesting that the experimental point for the largest ejection energy (possibly also at 95 keV incident energy, where no CDW-EIS results are available) may be inaccurate.

Figure 2 does not show experimental uncertainties as it is difficult to gauge them from Ref. [31]. However, the experimental data on the singly differential cross sections were

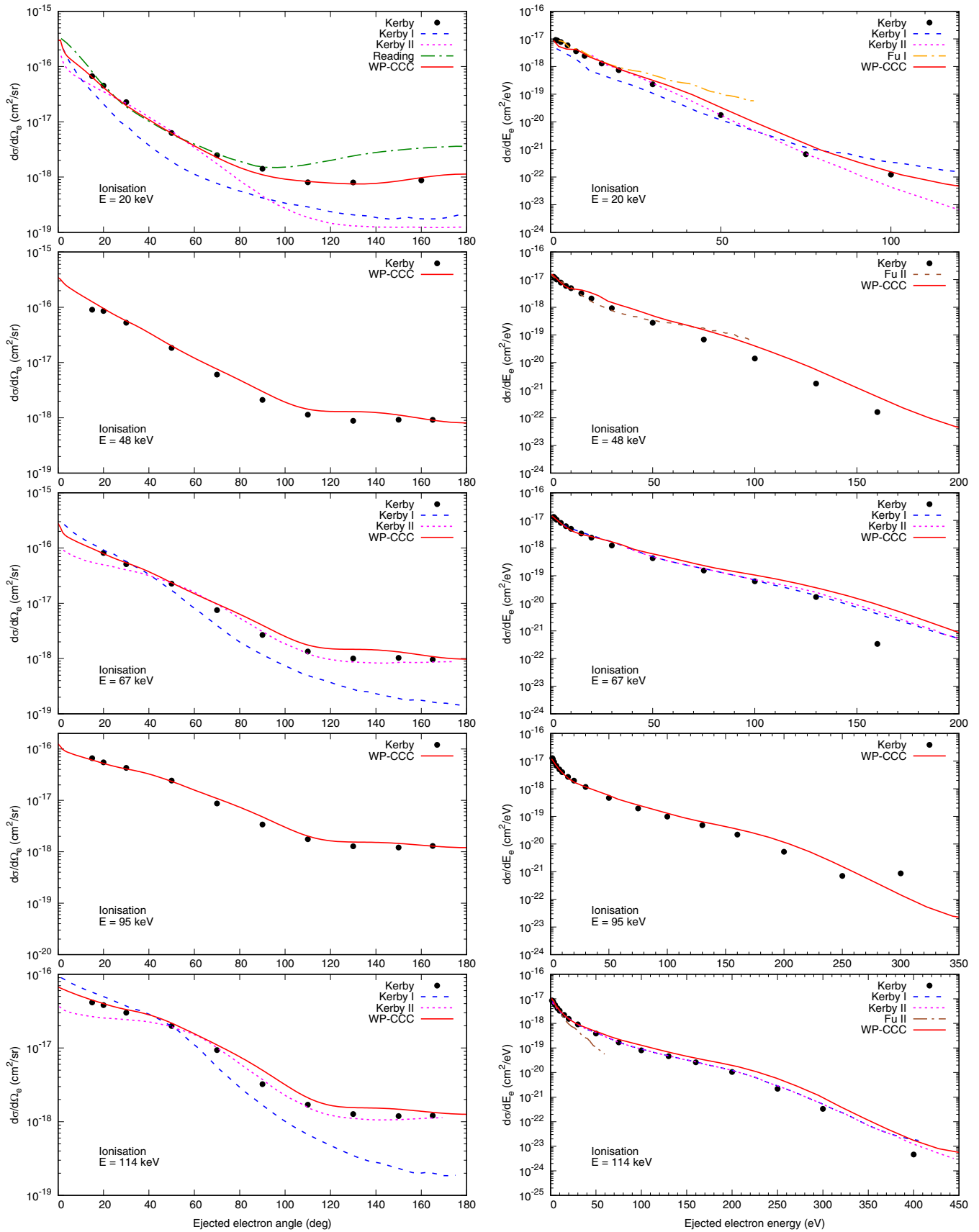


FIG. 2. Singly differential ionization cross sections (in the laboratory frame) as functions of electron ejection angle and energy. The experimental data: Kerby *et al.* [31]. The theoretical results: the present WP-CCC approach; the CTMC (I) and CDW-EIS (II) approaches by Kerby *et al.* [31]; the FHBS approach by Reading *et al.* [61], Fu [62] (I) and Fu *et al.* [63] (II).



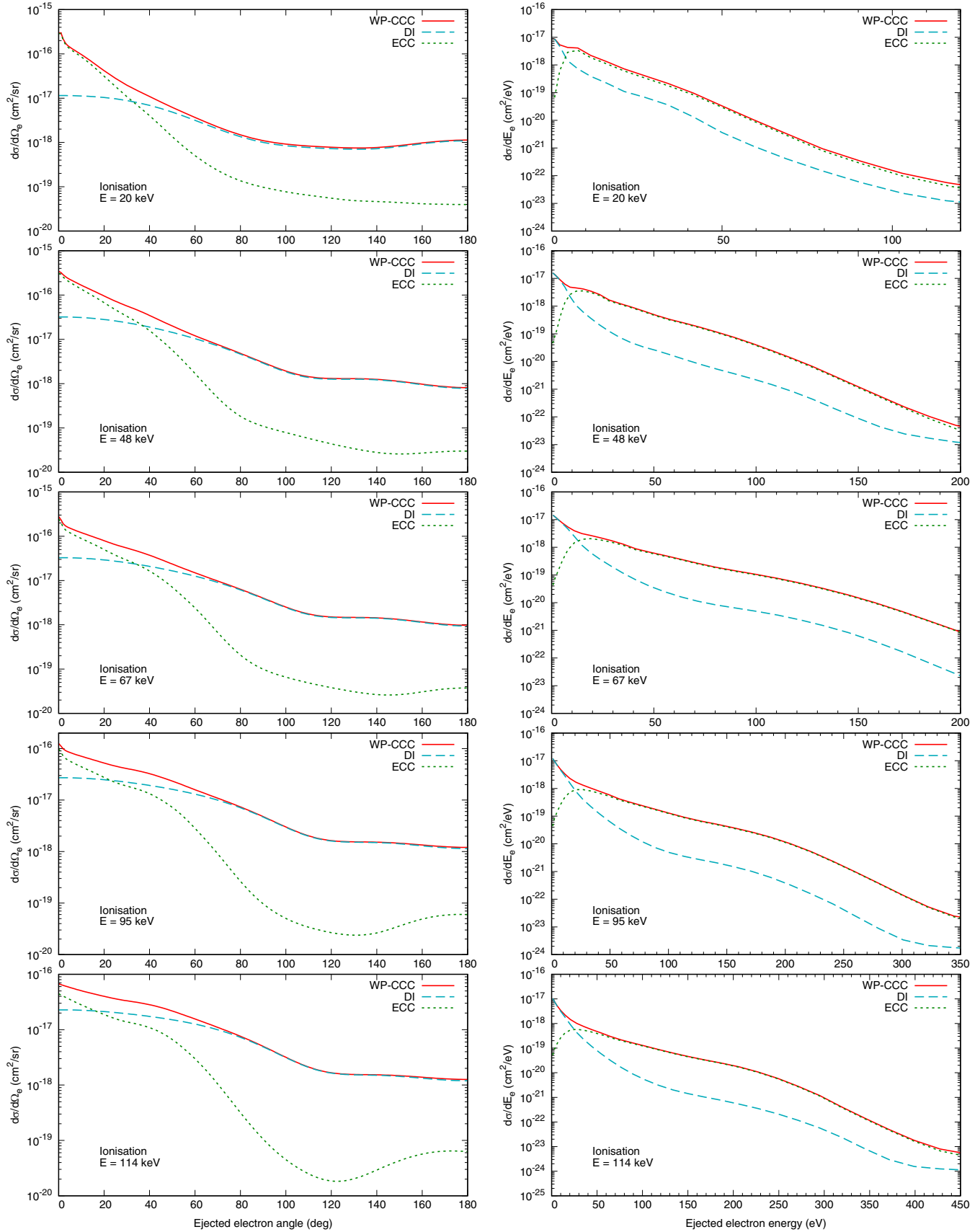


FIG. 3. Direct ionization and electron capture into continuum components of the singly differential ionization cross sections (in the laboratory frame) as functions of electron ejection angle and energy.

obtained by numerically integrating the experimental doubly differential cross section over angle or electron energy [31]. As mentioned in the associated work [64] the uncertainties in the corresponding doubly differential cross sections were 22% above 10 eV, increasing to 26% at 1.5 eV and to 50% or more at the very highest energies. Consequently, the uncertainties in the SDCS data are expected to be even larger.

Figure 3 shows the individual components of the SDCS representing direct ionization and electron capture into the continuum [see Eqs. (21) and (22) for the corresponding amplitudes] along with their sum. In the angular SDCS (left panels), ECC gives a dominant contribution when the electron is ejected in the forward direction indicating the electron travels with the projectile. As the ejection angle grows DI becomes dominant. Furthermore, the significance of ECC drops as the collision energy goes up. This indicates that at higher projectile energies the likelihood of charge exchange processes decreases. The SDCS in ejected electron energy shown in the right panels is dominated by the DI component when the electron is slow indicating the electron remains close to the target nucleus. However, when the ejected electron is more energetic, the SDCS is dominated by ECC suggesting that the electron travels closer to the scattered projectile.

#### IV. CONCLUSION

The two-center wave-packet convergent close-coupling approach was applied to calculate singly differential cross

sections for electron capture, direct scattering, and ionization in proton-hydrogen collisions at intermediate projectile energies. Convergent results obtained for the angular differential cross sections of elastic scattering, excitation and electron capture agree well with experiment. Fully convergent singly differential ionization cross sections in the ejected electron angle and in the ejected electron energy also agree well with available experiment. It is concluded that the two-center wave-packet convergent close-coupling approach is capable of providing a fairly accurate and complete differential picture of all processes taking place in proton-hydrogen collisions simultaneously. The distinct feature of the approach is that it gives a complete differential picture of all the interconnected processes at once, subject to the unitary principle.

Application of the method to other projectiles and multi-electron targets is underway. In particular, application of the method to proton-helium collisions may shed more light on the mechanism for electron capture discussed in Ref. [65]. According to this mechanism the electron capture takes place due to the emission of the second electron mainly in the backward direction.

#### ACKNOWLEDGMENTS

This work was supported by the Australian Research Council, the Pawsey Supercomputer Centre, and the National Computing Infrastructure. C. T. Plowman acknowledges support through an Australian Government Research Training Program Scholarship.

- 
- [1] R. Hemsworth, H. Decamps, J. Graceffa, B. Schunke, M. Tanaka, M. Dremel, A. Tanga, H. De Esch, F. Geli, J. Milnes *et al.*, *Nucl. Fusion* **49**, 045006 (2009).
  - [2] O. Marchuk, *Phys. Scr.* **89**, 114010 (2014).
  - [3] K. Heng and R. A. Sunyaev, *Astron. Astrophys.* **481**, 117 (2008).
  - [4] Dž. Belkić, *J. Math. Chem.* **47**, 1366 (2010).
  - [5] B. H. Bransden and M. R. C. McDowell, *Charge Exchange and the Theory of Ion-Atom Collisions* (Clarendon Press, Oxford, 1992).
  - [6] Dž. Belkić, I. Bray, and A. Kadyrov, *State-of-the-Art Reviews on Energetic Ion-Atom and Ion-Molecule Collisions* (World Scientific, Singapore, 2019).
  - [7] C. Illescas and A. Riera, *Phys. Rev. A* **60**, 4546 (1999).
  - [8] A. Jorge, L. F. Errea, C. Illescas, and L. Méndez, *Eur. Phys. J. D* **68**, 227 (2014).
  - [9] S. Borbély, J. Feist, K. Tókési, S. Nagele, L. Nagy, and J. Burgdörfer, *Phys. Rev. A* **90**, 052706 (2014).
  - [10] M. Baxter and T. Kirchner, *Phys. Rev. A* **93**, 012502 (2016).
  - [11] A. C. K. Leung and T. Kirchner, *Eur. Phys. J. D* **73**, 246 (2019).
  - [12] J. Kuang and C. D. Lin, *J. Phys. B* **29**, 1207 (1996).
  - [13] N. Toshima, *J. Phys. B* **30**, L131 (1997).
  - [14] N. Toshima, *Phys. Rev. A* **59**, 1981 (1999).
  - [15] T. G. Winter, *Phys. Rev. A* **80**, 032701 (2009).
  - [16] J. W. Gao, Y. Wu, J. G. Wang, N. Sisourat, and A. Dubois, *Phys. Rev. A* **97**, 052709 (2018).
  - [17] D. Jakimovski and R. K. Janev, *Eur. Phys. J. D* **73**, 175 (2019).
  - [18] H. Agueny, J. P. Hansen, A. Dubois, A. Makhoute, A. Taoutioui, and N. Sisourat, *At. Data Nucl. Data Tables* **129-130**, 101281 (2019).
  - [19] M. S. Pindzola and D. R. Schultz, *Phys. Rev. A* **77**, 014701 (2008).
  - [20] D. Tseliakhovich, C. M. Hirata, and K. Heng, *Mon. Notices Royal Astron. Soc.* **422**, 2357 (2012).
  - [21] A. Jorge, J. Suárez, C. Illescas, L. F. Errea, and L. Méndez, *Phys. Rev. A* **94**, 032707 (2016).
  - [22] Dž. Belkić, *Phys. Rev. A* **43**, 4751 (1991).
  - [23] Dž. Belkić, R. Gayet, and A. Salin, *Phys. Rep.* **56**, 279 (1979).
  - [24] R. D. Rivarola, P. D. Fainstein, and V. H. Ponce, *Phys. Scr.* **1989**, 101 (1989).
  - [25] I. B. Abdurakhmanov, A. S. Kadyrov, S. K. Avazbaev, and I. Bray, *J. Phys. B* **49**, 115203 (2016).
  - [26] I. B. Abdurakhmanov, A. S. Kadyrov, and I. Bray, *J. Phys. B* **49**, 03LT01 (2016).
  - [27] S. K. Avazbaev, A. S. Kadyrov, I. B. Abdurakhmanov, D. V. Fursa, and I. Bray, *Phys. Rev. A* **93**, 022710 (2016).
  - [28] I. B. Abdurakhmanov, A. S. Kadyrov, and I. Bray, *Phys. Rev. A* **94**, 022703 (2016).
  - [29] I. B. Abdurakhmanov, J. J. Bailey, A. S. Kadyrov, and I. Bray, *Phys. Rev. A* **97**, 032707 (2018).

- [30] I. B. Abdurakhmanov, A. S. Kadyrov, I. Bray, and K. Bartschat, *Phys. Rev. A* **96**, 022702 (2017).
- [31] G. W. Kerby, M. W. Gealy, Y.-Y. Hsu, M. E. Rudd, D. R. Schultz, and C. O. Reinhold, *Phys. Rev. A* **51**, 2256 (1995).
- [32] I. B. Abdurakhmanov, O. Erkilic, A. S. Kadyrov, I. Bray, S. K. Avazbaev, and A. M. Mukhamedzhanov, *J. Phys. B* **52**, 105701 (2019).
- [33] I. B. Abdurakhmanov, S. U. Alladustov, J. J. Bailey, A. S. Kadyrov, and I. Bray, *Plasma Phys. Controlled Fusion* **60**, 095009 (2018).
- [34] I. B. Abdurakhmanov, K. Massen-Hane, S. U. Alladustov, J. J. Bailey, A. S. Kadyrov, and I. Bray, *Phys. Rev. A* **98**, 062710 (2018).
- [35] J. Faulkner, I. B. Abdurakhmanov, S. U. Alladustov, A. S. Kadyrov, and I. Bray, *Plasma Phys. Controlled Fusion* **61**, 095005 (2019).
- [36] S. U. Alladustov, I. B. Abdurakhmanov, A. S. Kadyrov, I. Bray, and K. Bartschat, *Phys. Rev. A* **99**, 052706 (2019).
- [37] S. Chandrasekaran and G. Juckeland, *OpenACC for Programmers: Concepts and Strategies* (Addison-Wesley Professional, Boston, MA, 2017).
- [38] *CuSolver Library* (NVIDIA Corporation, Santa Clara, CA, 2018).
- [39] A. S. Kadyrov, I. Bray, A. M. Mukhamedzhanov, and A. T. Stelbovics, *Phys. Rev. Lett.* **101**, 230405 (2008).
- [40] A. S. Kadyrov, I. Bray, A. M. Mukhamedzhanov, and A. T. Stelbovics, *Ann. Phys.* **324**, 1516 (2009).
- [41] E. O. Alt and A. M. Mukhamedzhanov, *Phys. Rev. A* **47**, 2004 (1993).
- [42] A. M. Mukhamedzhanov, A. S. Kadyrov, and F. Pirlepesov, *Phys. Rev. A* **73**, 012713 (2006).
- [43] A. S. Kadyrov, J. J. Bailey, I. Bray, and A. T. Stelbovics, *Phys. Rev. A* **89**, 012706 (2014).
- [44] Comparative analysis of the coherent and incoherent combinations of the components was performed in Ref. [29]. It was shown that, for all practical purposes, the computationally less demanding incoherent combination can be used.
- [45] E. Rille, J. L. Peacher, E. Redd, T. J. Kvale, D. G. Seely, D. M. Blankenship, R. E. Olson, and J. T. Park, *Phys. Rev. A* **29**, 521 (1984).
- [46] J. T. Park, J. E. Aldag, J. L. Peacher, and J. M. George, *Phys. Rev. A* **21**, 751 (1980).
- [47] P. J. Martin, D. M. Blankenship, T. J. Kvale, E. Redd, J. L. Peacher, and J. T. Park, *Phys. Rev. A* **23**, 3357(R) (1981).
- [48] E. O. Alt, A. S. Kadyrov, and A. M. Mukhamedzhanov, *Phys. Rev. A* **60**, 314 (1999).
- [49] D. Dewangan and J. Eichler, *J. Phys. B* **17**, L541 (1984).
- [50] A. Henne, H. Ludde, A. Toepfer, T. Gluth, and R. Dreizler, *J. Phys. B* **26**, 3815 (1993).
- [51] A. S. Kadyrov, I. B. Abdurakhmanov, I. Bray, and A. T. Stelbovics, *Phys. Rev. A* **80**, 022704 (2009).
- [52] R. Potvliege, F. Furtado, and C. Joachain, *J. Phys. B* **20**, 1771 (1987).
- [53] V. Rodriguez, *J. Phys. B* **24**, L205 (1991).
- [54] T. G. Wong, M. Foster, J. Colgan, and D. H. Madison, *Eur. Phys. J.* **30**, 447 (2009).
- [55] V. Y. Lazur, V. Aleksiy, M. Karbovanets, M. Khoma, and S. Myhalyna, *Semicond. Phys. Quantum Electron. Optoelectron.* **22** 171 (2019).
- [56] N. Milojević, I. Mančev, D. Delibašić, and Dž. Belkić, *Phys. Rev. A* **102**, 012816 (2020).
- [57] L. H. Thomas, *Proc. Roy. Soc. A* **114**, 561 (1927).
- [58] H. Vogt, R. Schuch, E. Justiniano, M. Schulz, and W. Schwab, *Phys. Rev. Lett.* **57**, 2256 (1986).
- [59] N. Toshima and J. Eichler, *Phys. Rev. Lett.* **66**, 1050 (1991).
- [60] N. Toshima and J. Eichler, *Phys. Rev. A* **46**, 2564 (1992).
- [61] J. F. Reading, J. Fu, and M. J. Fitzpatrick, *Phys. Rev. A* **70**, 032718 (2004).
- [62] J. Fu, FHBS calculation of ionized electron angular and energy distribution following the p+H collision at 20 keV, Ph.D. thesis, Texas A&M University, 2004.
- [63] J. Fu, M. J. Fitzpatrick, J. F. Reading, and R. Gayet, *J. Phys. B* **34**, 15 (2001).
- [64] M. W. Gealy, G. W. Kerby, Y.-Y. Hsu, and M. E. Rudd, *Phys. Rev. A* **51**, 2247 (1995).
- [65] A. B. Voitkiv, B. Najjari, and J. Ullrich, [arXiv:0808.0590](https://arxiv.org/abs/0808.0590).